Variational Analysis of the Phenyl + O_2 and Phenoxy + O Reactions

Gabriel da Silva[†,‡] **and Joseph W. Bozzelli***[,†]

Department of Chemistry and Environmental Science, New Jersey Institute of Technology, Newark, New Jersey 07102, and Department of Chemical and Biomolecular Engineering, The University of Melbourne, Victoria 3010, Australia

Received: December 18, 2007; In Final Form: January 30, 2008

Variational transition state analysis was performed on the barrierless phenyl + O_2 and phenoxy + O association reactions. In addition, we also calculated rate constants for the related vinyl radical (C_2H_3) + O_2 and vinoxy radical (C_2H_3O) + O reactions and provided rate constant estimates for analogous reactions in substituted aromatic systems. Potential energy scans along the dissociating C−OO and CO−O bonds (with consideration of C−OO internal rotation) were obtained at the O3LYP/6-31G(d) density functional theory level. The CO−O and C−OO bond scission reactions were observed to be barrierless, in both phenyl and vinyl systems. Potential energy wells were scaled by G3B3 reaction enthalpies to obtain accurate activation enthalpies. Frequency calculations were performed for all reactants and products and at points along the potential energy surfaces, allowing us to evaluate thermochemical properties as a function of temperature according to the principles of statistical mechanics and the rigid rotor harmonic oscillator (RRHO) approximation. The low-frequency vibrational modes corresponding to R−OO internal rotation were omitted from the RRHO analysis and replaced with a hindered internal rotor analysis using O3LYP/6-31G(d) rotor potentials. Rate constants were calculated as a function of temperature (300−2000 K) and position from activation entropies and enthalpies, according to canonical transition state theory; these rate constants were minimized with respect to position to obtain variational rate constants as a function of temperature. For the phenyl + O_2 reaction, we identified the transition state to be located at a C−OO bond length of between 2.56 and 2.16 Å (300−2000 K), while for the phenoxy + O reaction, the transition state was located at a CO−O bond length of 2.00−1.90 Å. Variational rate constants were fit to a three-parameter form of the Arrhenius equation, and for the phenyl + O_2 association reaction, we found $k(T) = 1.860 \times 10^{13} T^{-0.217} \exp(0.358/T)$ (with k in cm^3 mol^{-1} s^{-1} and T in K); this rate equation provides good agreement with low-temperature experimental measurements of the phenyl + O_2 rate constant. Preliminary results were presented for a correlation between activation energy (or reaction enthalpy) and pre-exponential factor for heterolytic O−O bond scission reactions.

Introduction

Molecules containing the aromatic C6 benzene ring are ubiquitous in thermal reaction systems. Aromatic hydrocarbons such as benzene, toluene, xylene, and ethylbenzene form a significant component of petroleum-derived fuels, and much effort has been directed toward the development of kinetic models that accurately describe the reactions of these aromatic compounds in combustion systems and in the atmosphere. There is also great interest in the reactions of polyaromatic hydrocarbons (PAHs) in thermal systems, as PAHs are precursors to unwanted soot formation. Furthermore, the supertoxic dioxins, including polychlorinated dibenzofurans (PCDFs) and polychlorinated dibenzodioxins (PCDBs), contain aromatic backbones, and reactions at these aromatic sites are of importance in both the formation and the destruction of these toxins.

There is a clear requirement for accurate kinetic models describing the reactions of aromatic molecules, either as fuels or as reaction products and intermediates. An important step in the initial reactions of aromatic molecules is the abstraction of a phenyl C−H hydrogen atom. The phenyl C−H bond dissociation energy (BDE) is 113 kcal mol^{-1},[1] and at high to moderate temperatures, the phenyl hydrogen can be abstracted by O_2, as well as by active radical species including H and O atoms, CH_3 (and RCH_2), CN, OH, etc. Recently, several low-temperature pathways leading to phenyl (and methylphenyl) radical production via resonance-stabilized benzyl radicals also have been postulated.[2,3] Further reactions of the phenyl radical, and substituted phenyl radicals, in thermal systems therefore need to be considered. Especially important is the association of phenyl radicals with O_2; these reactions result in phenylperoxy adducts with ca. 50 kcal mol^{-1} of chemical activation energy,[2,3] and this energy can go into a variety of isomerization and dissociation reactions, ultimately leading to the destruction of the aromatic ring structure (through reactions including ring opening and C5 cyclization).[2−5] As with many radical + O_2 reactions, it is generally agreed that the phenyl + O_2 association proceeds without a barrier in the forward direction and with only a thermodynamic barrier (no intrinsic barrier) in the reverse direction. Such reactions are referred to as being barrierless.

Dissociation to the phenoxy radical + O atom is another important reaction of the phenylperoxy radical, with a chain-branching product set. This reaction is often considered to be barrierless. At moderate to high temperatures, the phenoxy radical will undergo unimolecular elimination of CO, yielding the C_5H_5 cyclopentadienyl radical.[6] The phenoxy radical is,

* Corresponding author. E-mail: bozzelli@njit.edu; tel.: (973) 596-3459; fax: (973) 596-3586.
† New Jersey Institute of Technology.
‡ The University of Melbourne.

10.1021/jp7118845 CCC: $40.75
Published on Web 03/19/2008

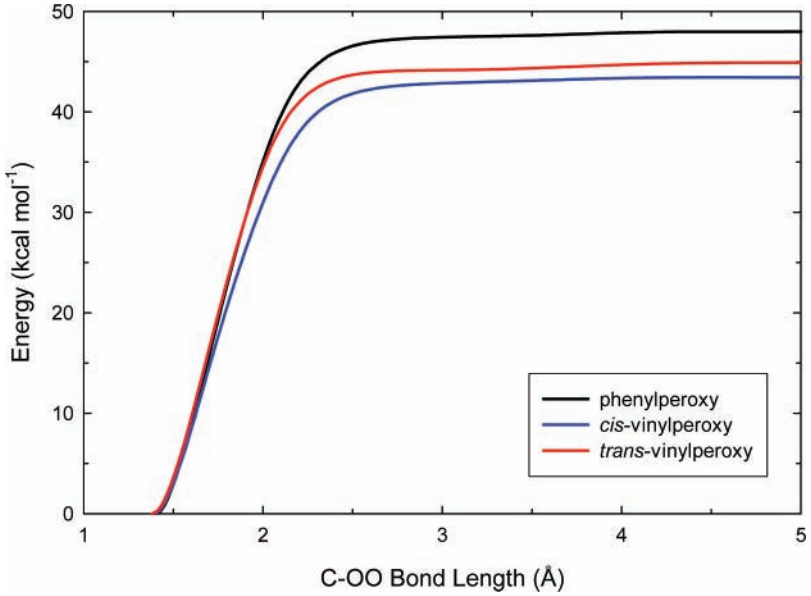

Figure 1. Potential energy surfaces for C−OO bond dissociation in the phenylperoxy radical and the *cis*- and *trans*-vinylperoxy radicals (reaction to phenyl/vinyl + O_2) calculated at the O3LYP/6-31G(d) level, scaled by G3B3 reaction enthalpies.

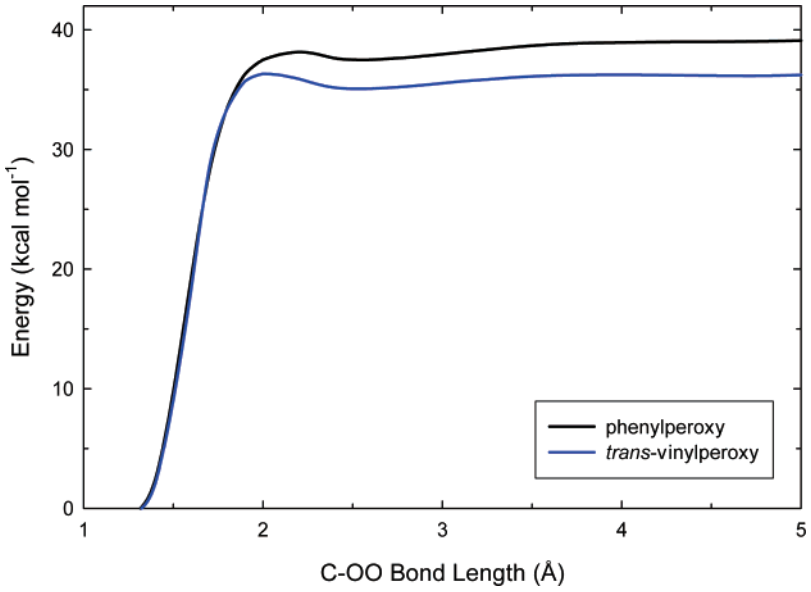

Figure 2. Potential energy surfaces for CO−O bond dissociation in the phenylperoxy and *trans*-vinylperoxy radicals (reaction to phenoxy/vinoxy + O). Calculated at the O3LYP/6-31G(d) level, scaled by G3B3 reaction enthalpies.

however, resonantly stabilized due to hyperconjugation of the oxyl radical moiety with the aromatic ring,[7] and as a result, the phenoxy radical and its substituted derivatives are relatively stable, and they often persist at low to moderate temperatures. These persistent free radicals (PFRs) are believed to be important in the formation of dioxins[8] and particulate matter[9] in post-combustion and atmospheric environments.

The vinyl (CH_2CH) and vinoxy (CH_2CHO) radicals also are important species in atmospheric and combustion chemistry. The reaction of vinyl radicals with O_2 has been studied extensively, both experimentally[10] and theoretically.[10g,11] The reaction predominantly produces CH_2O + HCO, with the chain-branching path to vinoxy + O important at higher temperatures, due to the entropy of the vinoxy transition state (i.e., high pre-exponential factor). It is well-known that bonds on phenylic and vinylic sites are similar in energy, where it has been suggested that vinylic bonds are ca. 3 kcal mol^{-1} weaker than similar phenylic bonds.[7,12] As such, the thermodynamics and kinetics of vinyl + O_2 and vinoxy + O association should mirror those observed in the analogous phenylic reactions. As with aromatic hydrocarbons, the vinyl radical also is important in PAH formation,[13] through reactions with species such as vinylacetylene[13a] and 1,3-butadiene.[13b] The resonance-stabilized vinoxy radical can be formed by C−H hydrogen abstraction in acetaldehyde (BDE = 95.5 kcal mol^{-1})[14] and O−H hydrogen abstraction in vinyl alcohol (BDE = 85.2 kcal mol^{-1}).[12] Both acetaldehyde and vinyl alcohol are important intermediates in a variety of thermal processes, including the combustion of ethanol;[15] the recent surge of interest in bioethanol as a renewable fuel places heightened importance on the reactions of acetaldehyde and vinyl alcohol.

Relatively little kinetic information is available on the phenyl + O_2 and phenoxy + O (and related) reactions, in spite of their importance. This is due in part to the difficulties associated with studying these reactions at moderate temperatures and above, where the phenylperoxy and phenoxy radicals readily decompose to further reaction products. There are two measurements of the phenyl + O_2 rate constant at low temperatures, to our

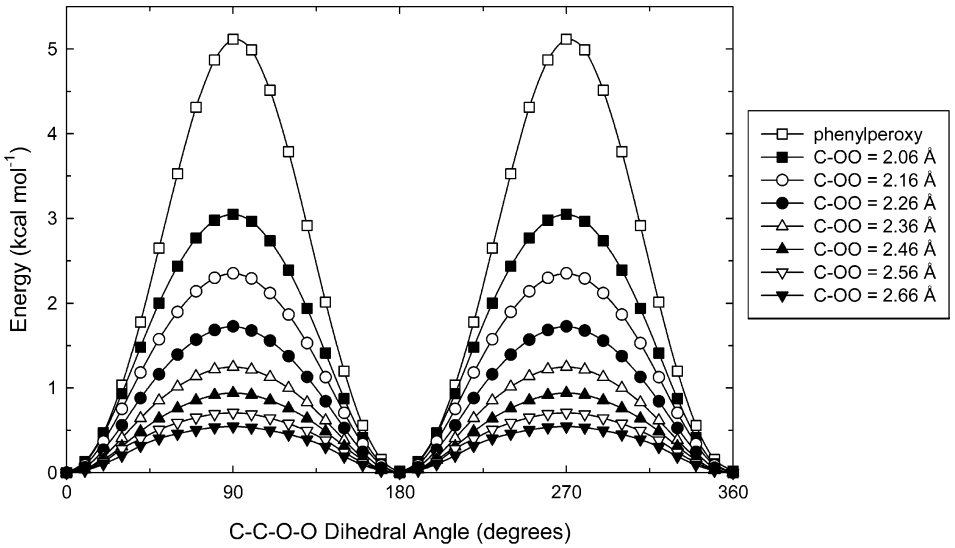

Figure 3. Internal rotor potentials in the phenylperoxy radical and in the phenyl−OO transition state geometries from O3LYP/6-31G(d) calculations.

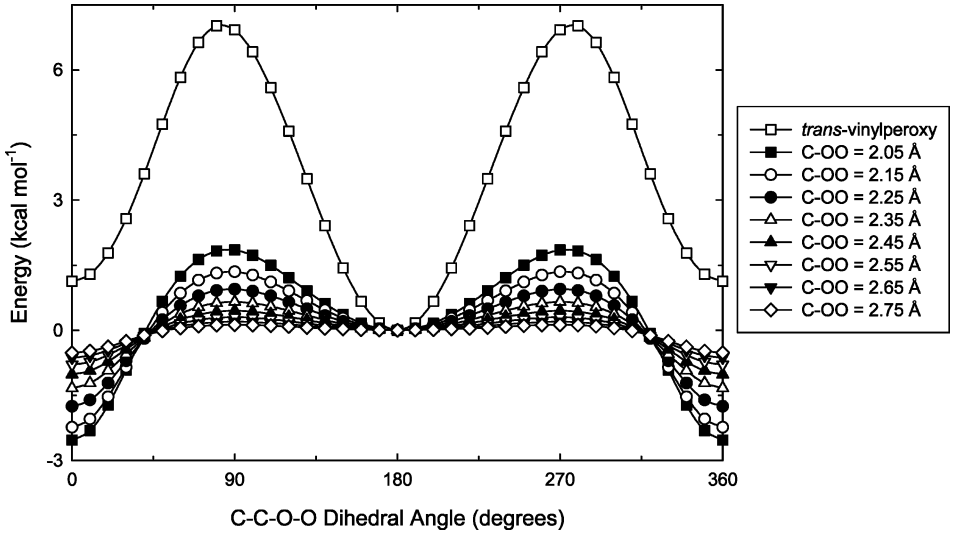

Figure 4. Internal rotor potentials in the vinylperoxy radical and in the vinyl−OO transition state geometries from O3LYP/6-31G(d) calculations. Energies relative to *trans*-vinylperoxy.

knowledge. Yu and Lin[16] measured $k = 10^{-11.00\pm0.08}\exp(+161 \pm 66/T)$ cm^3 molecule^{-1} s^{-1} for $T = 297-473$ K. The rate of reaction was studied at 20−80 Torr and was reported to be pressure independent; the results were assumed to be effectively in the high-pressure limit, on the basis of preliminary RRKM calculations. Yu and Lin observed a small negative temperature dependence, equivalent to an activation energy of −0.32 kcal mol^{-1}. Schaugg et al.[17] also measured the rate of phenyl + O_2 association and found $k = 3.8 \times 10^{11}\exp(-290/T)$ cm^3 molecule^{-1} s^{-1} for $T = 418-815$ K at around 0.7 mbar. The rate expression of Schaugg et al. is in relatively good agreement with that of Yu and Lin but shows a small positive temperature dependence ($E_a = +0.58$ kcal mol^{-1}). Schaugg et al. noted that wall effects were relatively large in reactions of the phenyl radical, especially at lower temperatures, further contributing to the uncertainty of the experimental measurements.

The barrierless phenyl + O_2 and phenoxy + O reactions are excellent candidates for a theoretical study, due to difficulties associated with studying these reactions experimentally. Theoretically, high-pressure limit rate constants can be calculated as a function of temperature from the enthalpy of activation ($\Delta H^{\ddagger}(T)$) and entropy of activation ($\Delta S^{\ddagger}(T)$), according to canonical transition state theory (eq 1). However, to rigorously treat barrierless reactions, we must consider the variational nature of the transition state. At low temperatures, where enthalpic considerations dominate, the transition state will be loose, with the forward barrier close to the entrance barrier height. At higher temperatures, entropic effects constitute a larger contribution to the free energy of activation. Transition state entropies become smaller (less favorable) as the cleaving bond shortens and the moments of inertia reduce, and therefore, at higher temperatures, we find a tighter transition state. The variational nature of the transition state in barrierless reactions is thought to be responsible for their often-observed complex temperature dependence[18]

$$k(T) = \frac{\sigma k_b T}{h}\exp\left(\frac{\Delta S^{\ddagger}}{R}\right)\exp\left(\frac{-\Delta H^{\ddagger}}{RT}\right) \quad (1)$$

We studied the phenyl + O_2 and phenoxy + O reactions according to variational transition state theory, using density functional theory (DFT) and ab initio methods. The results of this study will be useful in modeling the combustion kinetics of aromatic fuels such as benzene, toluene, xylene, and ethylbenzene and also for modeling the formation and destruction of PAHs and dioxins in thermal systems. Additionally, we

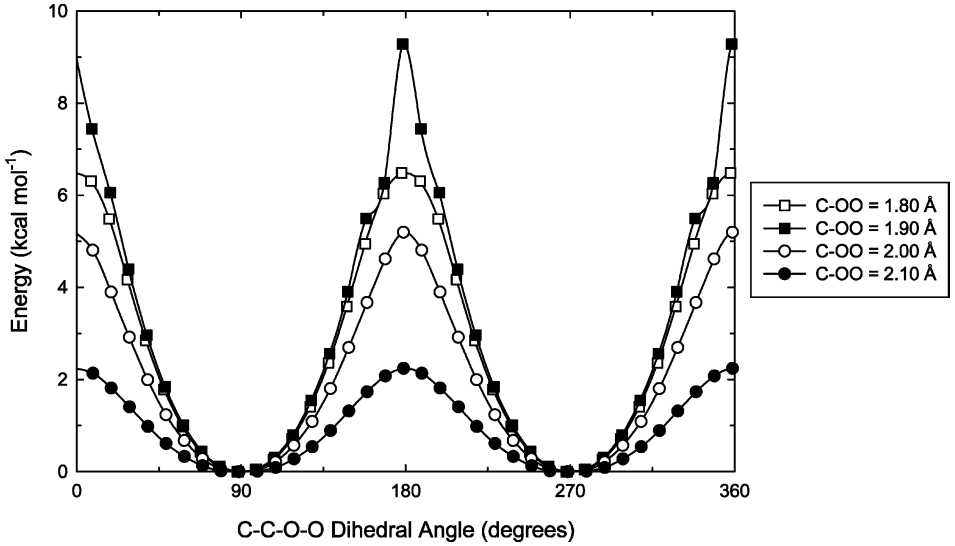

Figure 5. Internal rotor potentials in the phenoxy−O transition state geometries from O3LYP/6-31G(d) calculations.

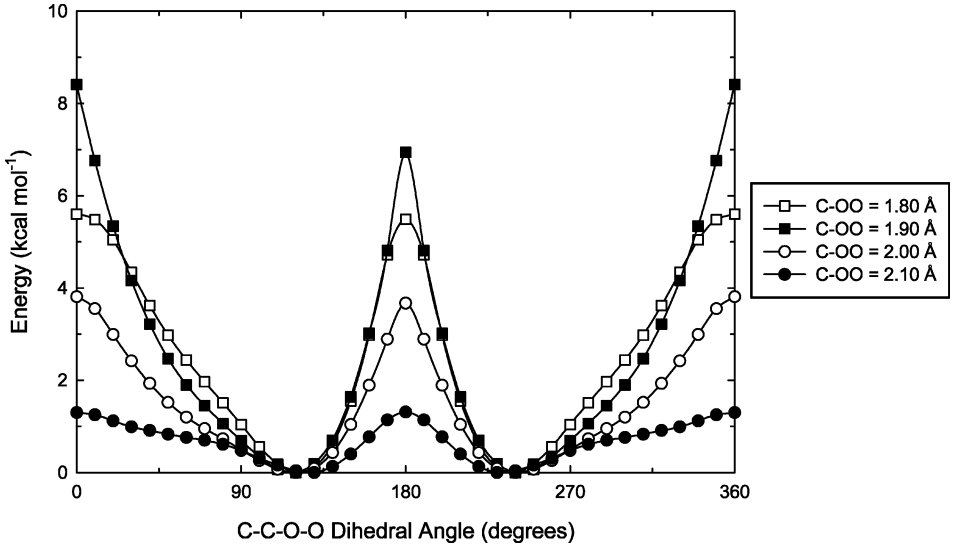

Figure 6. Internal rotor potentials in the vinoxy−O transition state geometries from O3LYP/6-31G(d) calculations. Energies relative to *trans*-vinylperoxy.

present rate constants for the analogous vinyl + O_2 and vinoxy + O reactions, which, for example, will be important in the combustion of the important biofuel ethanol and also in PAH formation.

Materials and Methods

Potential energy surfaces (PES) were obtained for dissociation of the C−OO and CO−O bonds in the phenylperoxy and vinylperoxy radicals from ab initio and DFT calculations. Relaxed potential energy scans were performed along the dissociating bond lengths at 0.1 Å intervals using the hybrid DFT method O3LYP,[19] with the 6-31G(d) basis set. The O3LYP DFT method gives a comparable or better performance than the popular B3LYP method for barrier heights and atomization energies in organic reaction systems.[20] The resultant O3LYP/6-31G(d) PES were then scaled to provide a more accurate well-depth, using reaction enthalpies calculated with the G3B3 composite theoretical method;[21] scaling factors were between 0.88 and 1.13. Frequency calculations were performed on optimized geometries along the C−OO and CO−O PES. All transition state structures utilized in our VTST calculations returned a single imaginary frequency with the mode of vibration corresponding to C−OO or CO−O bond cleavage. All DFT and ab initio calculations were performed using the Gaussian 03 program.[22] Relative energies and scaled enthalpies as a function of the C−OO and CO−O distances for all systems are provided as Supporting Information.

Thermochemical properties (including $S°$, C_P, $\Delta_f H°$, and $\Delta_f G°$) were calculated as a function of temperature from 300 to 2000 K for all species and transition states, from statistical mechanical principles. All thermochemical and kinetic parameters were calculated using the ChemRate program.[23] Vibrational and translational frequencies were modeled using the rigid rotor harmonic oscillator (RRHO) approximation. Low-frequency vibrations corresponding to C−OO internal rotation were omitted from the RRHO analysis and treated as hindered internal rotations. In this treatment, internal rotor potentials were calculated at the O3LYP/6-31G(d) level, to determine the barrier to rotation, the rotational symmetry, and the number of rotational minima. ChemRate determines moments of inertia for internal rotors based upon molecular structure and connectivity;[24] moments of inertia are subsequently employed in evaluating the contribution of the internal rotor to the molecule's partition function.[25] For comparative purposes, variational rate constants

TABLE 1: Rate Constants (k, cm^3 mol^{-1} s^{-1}) as a Function of Temperature and Position for Barrierless Phenyl + O_2 Association Reaction[a]

	C_6H_5−OO distance (Å)						
temp (K)	2.06	2.16	2.26	2.36	2.46	2.56	2.66
300	3.23×10^{18}	1.08×10^{16}	3.73×10^{14}	6.88×10^{13}	2.91×10^{13}	**1.87×10^{13}**	2.09×10^{13}
400	4.69×10^{16}	7.67×10^{14}	7.32×10^{13}	2.47×10^{13}	1.49×10^{13}	**1.17×10^{13}**	1.47×10^{13}
500	3.97×10^{15}	1.68×10^{14}	2.94×10^{13}	1.42×10^{13}	1.05×10^{13}	**9.35×10^{12}**	1.26×10^{13}
600	8.06×10^{14}	6.42×10^{13}	1.67×10^{13}	1.02×10^{13}	8.64×10^{12}	**8.33×10^{12}**	1.17×10^{13}
700	2.67×10^{14}	3.33×10^{13}	1.15×10^{13}	8.25×10^{12}	**7.71×10^{12}**	7.87×10^{12}	1.14×10^{13}
800	1.19×10^{14}	2.08×10^{13}	8.86×10^{12}	**7.19×10^{12}**	7.22×10^{12}	7.67×10^{12}	1.14×10^{13}
900	6.52×10^{13}	1.47×10^{13}	7.36×10^{12}	**6.57×10^{12}**	6.96×10^{12}	7.64×10^{12}	1.16×10^{13}
1000	4.07×10^{13}	1.13×10^{13}	6.42×10^{12}	**6.18×10^{12}**	6.84×10^{12}	7.70×10^{12}	1.18×10^{13}
1100	2.80×10^{13}	9.19×10^{12}	**5.80×10^{12}**	5.94×10^{12}	6.81×10^{12}	7.82×10^{12}	1.22×10^{13}
1200	2.07×10^{13}	7.81×10^{12}	**5.38×10^{12}**	5.79×10^{12}	6.83×10^{12}	7.98×10^{12}	1.25×10^{13}
1300	1.62×10^{13}	6.86×10^{12}	**5.08×10^{12}**	5.70×10^{12}	6.90×10^{12}	8.18×10^{12}	1.29×10^{13}
1400	1.31×10^{13}	6.17×10^{12}	**4.86×10^{12}**	5.66×10^{12}	7.00×10^{12}	8.40×10^{12}	1.34×10^{13}
1500	1.11×10^{13}	5.66×10^{12}	**4.71×10^{12}**	5.66×10^{12}	7.12×10^{12}	8.63×10^{12}	1.38×10^{13}
1600	9.54×10^{13}	5.27×10^{12}	**4.60×10^{12}**	5.68×10^{12}	7.26×10^{12}	8.88×10^{12}	1.43×10^{13}
1700	8.42×10^{12}	4.97×10^{12}	**4.52×10^{12}**	5.72×10^{12}	7.41×10^{12}	9.14×10^{12}	1.48×10^{13}
1800	7.56×10^{12}	4.74×10^{12}	**4.46×10^{12}**	5.77×10^{12}	7.57×10^{12}	9.41×10^{12}	1.53×10^{13}
1900	6.88×10^{12}	4.55×10^{12}	**4.43×10^{12}**	5.84×10^{12}	7.74×10^{12}	9.68×10^{12}	1.58×10^{13}
2000	6.35×10^{12}	**4.40×10^{12}**	4.41×10^{12}	5.91×10^{12}	7.92×10^{12}	9.96×10^{12}	1.63×10^{13}

[a] Variational rate constant at each temperature is in bold.

TABLE 2: Rate Constants (k, cm^3 mol^{-1} s^{-1}) as a Function of Temperature and Position for Barrierless Phenoxy + O Association Reaction[a]

	C_6H_5O−O distance (Å)			
temp (K)	1.8	1.9	2.0	2.1
300	8.03×10^{16}	8.47×10^{14}	**2.37×10^{14}**	2.66×10^{14}
400	5.91×10^{15}	2.05×10^{14}	**9.52×10^{13}**	1.30×10^{14}
500	1.25×10^{15}	8.87×10^{13}	**5.65×10^{13}**	8.66×10^{13}
600	4.52×10^{14}	5.15×10^{13}	**4.07×10^{13}**	6.67×10^{13}
700	2.21×10^{14}	3.54×10^{13}	**3.26×10^{13}**	5.58×10^{13}
800	1.30×10^{14}	**2.69×10^{13}**	2.79×10^{13}	4.89×10^{13}
900	8.72×10^{13}	**2.20×10^{13}**	2.49×10^{13}	4.43×10^{13}
1000	6.35×10^{13}	**1.88×10^{13}**	2.29×10^{13}	4.09×10^{13}
1100	4.93×10^{13}	**1.66×10^{13}**	2.14×10^{13}	3.85×10^{13}
1200	4.00×10^{13}	**1.51×10^{13}**	2.04×10^{13}	3.65×10^{13}
1300	3.36×10^{13}	**1.40×10^{13}**	1.95×10^{13}	3.50×10^{13}
1400	2.91×10^{13}	**1.31×10^{13}**	1.89×10^{13}	3.37×10^{13}
1500	2.57×10^{13}	**1.24×10^{13}**	1.84×10^{13}	3.27×10^{13}
1600	2.30×10^{13}	**1.19×10^{13}**	1.80×10^{13}	3.18×10^{13}
1700	2.08×10^{13}	**1.14×10^{13}**	1.75×10^{13}	3.08×10^{13}
1800	1.93×10^{13}	**1.11×10^{13}**	1.73×10^{13}	3.04×10^{13}
1900	1.79×10^{13}	**1.08×10^{13}**	1.71×10^{13}	2.98×10^{13}
2000	1.68×10^{13}	**1.06×10^{13}**	1.69×10^{13}	2.93×10^{13}

[a] Variational rate constant at each temperature is in bold.

also were determined where C−OO internal rotation was treated as (i) a vibrational frequency and (ii) a free internal rotor.

Calculated thermochemical properties were used to determine high-pressure limit rate constants as a function of temperature (T) and position (z), $k(T,z)$, for the reverse dissociation reactions. Rate constants for the forward association reactions then were obtained according to the principle of microscopic reversibility, using calculated equilibrium constants. Forward and reverse rate constants were minimized at each temperature to obtain the variational rate constant. Variational $k(T)$ values were fit to an empirical three-parameter form of the Arrhenius equation (eq 2) to obtain the rate parameters E_a, A', and n

$$k(T) = A'T^n \exp\left(\frac{-E_a}{RT}\right) \qquad (2)$$

For the analogous reactions in substituted aromatic systems (including the methylphenyl and methylphenoxy radicals), rate constants were estimated using the phenyl and phenoxy systems but were adjusted for loss of symmetry (C_{2v} point group symmetry in phenyl and phenoxy vs C_1 symmetry in the substituted equivalents). This has the effect of doubling the forward (association) rate constants.

Results and Discussion

PES. Scaled O3LYP/6-31G(d) PES are presented in Figure 1 for the phenyl and vinyl + O_2 reactions and in Figure 2 for the phenoxy and vinoxy + O reactions. For the vinyl + O_2 reaction, we illustrated minimum energy pathways for the addition of O_2 in both cis and trans conformations. The phenyl + O_2 and phenoxy and vinoxy + O reactions feature two degenerate pathways, and this is accounted for in our rate constant calculations.

In Figure 1, we find that the three C−OO bond dissociation processes follow very similar PES. The shallowest potential energy well is provided by *cis*-vinylperoxy (44.0 kcal mol^{-1}), which is ca. 1 kcal mol^{-1} less stable than *trans*-vinylperoxy (44.9 kcal mol^{-1}). The phenyl + O_2 reaction exhibits the deepest energy well (48.6 kcal mol^{-1}). All three bond dissociation processes are essentially barrierless but demonstrate an almost imperceptible potential energy minima at around 3.0−3.5 Å, corresponding to the formation of a weak van der Waals complex (the van der Waals well).

PES for dissociation of the phenoxy−O and vinoxy−O bonds are provided in Figure 2. Here, we only consider the low-energy *trans*-vinylperoxy → vinoxy + O reaction (this is justified next). Again, the bond dissociation processes in the phenyl and vinyl systems are relatively similar, with a well depth of 40.3 kcal mol^{-1} for phenoxy + O and 37.2 kcal mol^{-1} for vinoxy + O. We now find significantly tighter transition states (as compared to C−OO bond dissociation), with maxima occurring at around 2.0 Å versus 2.5 Å; this should yield less-favorable pre-exponential factors. Furthermore, we detect significantly deeper van der Waals wells, especially for the vinoxy + O association reaction. The vinoxy + O reaction also exhibits a relatively well-defined transition state structure; however, the transition state energy is still below that of the entrance channel, due to the formation of the van der Waals complex (ca. 2 kcal mol^{-1}). We note that in the CO−O bond dissociation systems, formation of the van der Waals complex may become the rate-limiting process at lower temperatures (ca. 300 K and below).[18b]

Internal Rotor Potentials. Internal rotor potentials were calculated at the O3LYP/6-31G(d) level for the phenylperoxy

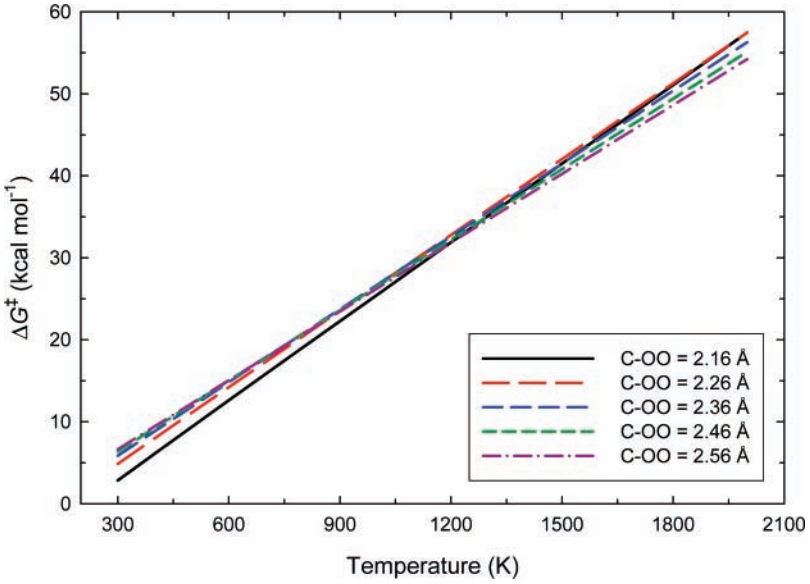

Figure 7. Free energy of activation for the barrierless phenyl + O_2 → phenylperoxy association reaction vs temperature for the five contributing transition state structures.

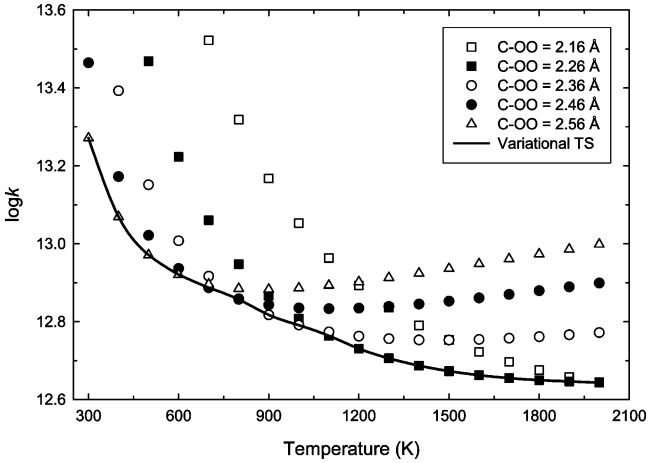

Figure 8. Calculated high-pressure limit rate constants (k, cm^3 mol^{-1} s^{-1}) vs temperature for the barrierless phenyl + O_2 → phenylperoxy association reaction. Solid line indicates the minimum variational rate constant.

radical and for the transition state geometries corresponding to C−OO and CO−O bond cleavage. The effect of treating C−OO and CO−O internal rotation as a hindered rotor, or as a free rotor or vibrational frequency, is examined later in the manuscript.

The phenylperoxy radical rotor potential is depicted in Figure 3, along with the rotor potentials in the phenyl + O_2 transition states. Figure 3 demonstrates that the phenyl−OO internal rotor has a two-fold barrier and decreases uniformly with increasing C−OO bond length. In the fully optimized phenylperoxy radical, the barrier to internal rotation is 5.1 kcal mol^{-1}. Similar calculations were performed for the vinyl system, with the results displayed in Figure 4 (relative to *trans*-vinylperoxy). The barrier to rotation is of a similar magnitude, and again, we find that this barrier decreases with increasing C−OO bond length. In the equilibrium vinylperoxy structures, we identify *trans*-vinylperoxy as being the most stable conformer (by 0.9 kcal mol^{-1} at the G3B3 level). However, as the C−OO bond length is stretched, the cis conformer becomes the most stable. This results in the cis channel for vinyl + O_2 association being kinetically more favorable, as we later demonstrate. The barrier for cis/trans isomerization in the *trans*-vinylperoxy radical is calculated to be 7.0 kcal mol^{-1} (or 5.9 kcal mol^{-1} in *cis*-vinylperoxy), in relative agreement with the rotational barrier for the phenylperoxy radical. The cis/trans isomerization process in the vinylperoxy radical has been considered several times in the scientific literature. Yang et al.[10g] found the trans conformer of the vinylperoxy radical to be more stable than the cis conformer by 1.3 kcal mol^{-1}, from B3LYP calculations, with a rotational barrier of 5.8 kcal mol^{-1}. Mebel et al.[11e] also studied cis/trans isomerization in the vinylperoxy radical using computational methods. They found the trans conformer to be more stable than the cis conformer by 1.2 kcal mol^{-1}, with the barrier for rotational isomerization being 6.1 kcal mol^{-1}.

In Figure 5, we present rotor potentials for the phenoxy + O transition states. Here, we find that the barrier to phenyl−OO internal rotation peaks at a CO−O bond of around 1.9 Å. We also find that the phenoxy + O transition states exhibit local minima in the gauche conformation, while the phenylperoxy radical and the phenyl + O_2 transition state geometries are all planar (C_s). Rotor potentials in the vinoxy + O association process are shown in Figure 6, and very similar results to the phenoxy + O system were obtained.

Variational Rate Constants. Rate constants were calculated as a function of temperature and position along the PES for each of the association reactions, and the results are presented in matrix form in Tables 1 and 2 for the phenyl + O_2 and phenoxy + O reactions, respectively. Rate constants for the other reactions are presented in the Supporting Information. In Tables 1 and 2, the minimum rate constant (which denotes the location of the transition state) at each temperature is highlighted.

For the phenyl + O_2 association reaction, we find that the transition state occurs at a C−OO bond length of 2.56 Å at 300 K, decreasing to 2.16 Å at 2000 K. For phenoxy + O, we find a tighter and less variable transition state, where the CO−O bond length is 2.00 Å at 300 K and 1.90 Å at 2000 K. Similar results were obtained for the vinyl systems, in terms of transition state structure as a function of temperature. Association rate constants are, however, considerably larger for the vinyl + O_2 reaction, as compared to phenyl + O_2. Transition states for the reverse (dissociation) reactions occur at the same position

TABLE 3: Empirical Rate Parameters (A', n, E_a) for Forward and Reverse R• + O_2 and RO• + O Reactions, Determined via VTST[a]

	A' (cm^3 mol^{-1} s^{-1})	n	E_a (kcal mol^{-1})
phenyl + O_2 → phenylperoxy	1.860×10^{13}	−0.217	−0.711
phenylperoxy → phenyl + O_2	6.360×10^{19}	−1.372	48.740
phenoxy + O → phenylperoxy	2.810×10^{13}	−0.197	−1.935
phenylperoxy → phenoxy + O	1.270×10^{15}	−0.246	38.536
R-phenyl + O_2 → *R*-phenylperoxy[b]	3.720×10^{13}	−0.217	−0.711
R-phenylperoxy → *R*-phenyl + O_2[b]	6.360×10^{19}	−1.372	48.740
R-phenoxy + O → *R*-phenylperoxy[b]	5.620×10^{13}	−0.197	−1.935
R-phenylperoxy → *R*-phenoxy + O[b]	1.270×10^{15}	−0.246	38.536
vinyl + O_2 → *cis*-vinylperoxy	2.340×10^{12}	−0.072	−0.985
cis-vinylperoxy → vinyl + O_2	2.710×10^{18}	−0.993	43.890
vinyl + O_2 → *trans*-vinylperoxy	2.180×10^{12}	−0.012	−0.686
trans-vinylperoxy → vinyl + O_2	7.900×10^{17}	−0.834	44.995
vinyl + O_2 → vinylperoxy (total)	3.850×10^{12}	−0.020	−0.860
vinylperoxy → vinyl + O_2 (total)	9.300×10^{17}	−0.777	43.925
vinoxy + O → *trans*-vinylperoxy (300−800 K)	2.070×10^{11}	0.344	−0.956
trans-vinylperoxy → vinoxy + *O*	1.380×10^{13}	0.236	36.516

[a] $k = A'T^n \exp(-E_a/RT)$. High-pressure limit rate parameters. [b] Representative of substituted aromatics, including alkyl benzenes (toluene, xylene, etc.) and polyaromatic hydrocarbons.

(vs T) as the forward (association) reactions, in accord with the principle of microscopic reversibility.

The variational nature of the phenyl + O_2 transition state is further illustrated in Figures 7 and 8. In Figure 7, the free energy of activation for this reaction is plotted as a function of temperature for each of the contributing transition state structures, while in Figure 8, the $k(T)$ values obtained with each transition state are presented, along with the limiting variational rate constant. In Figure 7, we readily observe that the maximum free energy barrier moves to the looser transition state structures at lower temperatures, segueing to the tighter transition states at higher temperatures. This results in the variational behavior observed in Figure 8.

Empirical rate parameters (A', n, E_a), as defined in eq 2, were fit to calculated rate constants for each of the studied reactions, according to a least-squares minimization in log $k(T)$. The results are presented in Table 3. From Table 3, we observe that the activation energies for the C−OO and CO−O dissociation reactions are close to the reaction enthalpies for these reactions. For the barrierless association reactions, we find small negative activation energies, in the range of −1.9 to −0.7 kcal mol^{-1}. Figure 9 shows a plot of the calculated variational rate constants for the barrierless phenyl and vinyl + O_2 and phenoxy and vinoxy + O association reactions.

Internal Rotor Treatment. Our calculations treat internal rotation about C−OO bonds as hindered rotations. To examine the effect of this internal rotational mode, variational rate constants also have been calculated where the C−OO internal rotor is treated as a vibrational frequency and as a free internal rotation. In Figure 10, we present variational rate constants for the phenyl + O_2 and phenoxy + O reactions obtained with each of the three internal rotor treatments. In both cases, we find that treatment of the internal rotor as a vibration and as a free rotor seems to provide the limiting cases to the hindered internal rotor analysis, as one would expect. For the phenyl + O_2 reaction, we find that at low temperatures the hindered rotor rate constants approach the free rotor values, while at higher temperatures, they approach the RRHO rate constants. This is somewhat counterintuitive but is a result of the variational nature of the transition state. At low temperatures, the transition state is loose, with a low barrier for internal rotation (ca. 0.5−1 kcal mol^{-1}), and the internal rotor is approximated as a free rotor. At higher temperatures, the transition state moves to a tighter geometry, with a larger barrier to internal rotation (ca. 2 kcal mol^{-1}), and the hindered rotor treatment provides a rate constant somewhere between the free rotor and the vibrational values. With the phenoxy + O reaction, the transition state is less variational and exhibits a large barrier for internal rotation (5−10 kcal mol^{-1}). We therefore found more classical behavior, where the hindered rotor rate constants approach the RRHO values at low temperatures and the free rotor values at high temperatures. We also noticed that the RRHO and free rotor rate constants converge at low temperatures.

Three-Dimensional PES. In this study, we focused on a two-dimensional treatment of the PES for the accurate determination of barrierless rate constants, with one spatial dimension describing bond dissociation and the other describing internal rotation. We constructed three-dimensional PES (two spatial dimensions and one energetic dimension) for the vinyl + O_2 and vinoxy + O reaction processes, and these are presented here as Figures 11 and 12, respectively. These figures illustrate the effect of both bond dissociation and internal rotation on molecular energy and help to illuminate the minimum energy pathway relative to the local and global minima.

For the vinyl + O_2 association (Figure 11), we observed two discrete reaction channels—one for cis addition and one for trans addition. While the *trans*-vinylperoxy radical is more stable than *cis*-vinylperoxy, the cis transition states become more stable for C−OO bond lengths of around 1.65 Å and greater. This results in the cis addition channel being more rapid than the trans channel at all but low temperatures. Given the low barrier for internal rotation in the vinylperoxy radical, this species should achieve thermal equilibrium on the time scales required for further reaction of the activated adduct, and the total vinyl + O_2 reaction rate is reported as the sum of the two separate channels.

In the vinoxy + O association reaction, depicted in Figure 12, we observed only one unique reaction channel. This is a result of the vinylperoxy minima moving from a planar to a gauche geometry as the CO−O bond is stretched, as we saw in Figure 6. The vinoxy + O association therefore proceeds with the oxygen atom approaching gauche to the radical, via two degenerate pathways. The minimum energy pathway then takes the vinylperoxy complex toward only the more stable trans conformation. The vinoxy + O → *cis*-vinylperoxy reaction demonstrates a higher energy second-order reaction pathway and is not expected to be important relative to the *trans*-vinylperoxy channels.

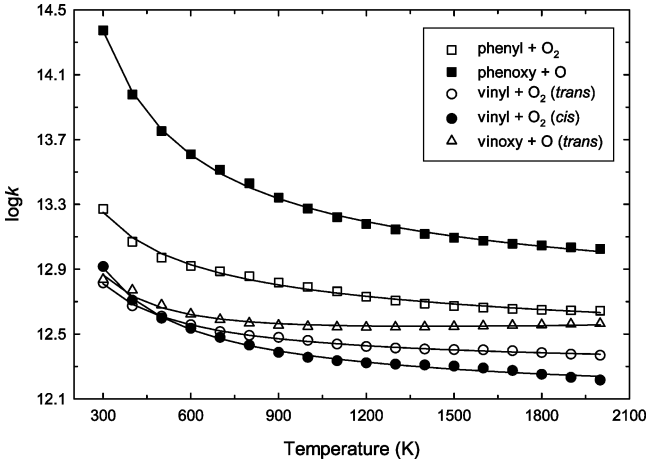

Figure 9. Calculated high-pressure rate constants (k, cm^3 mol^{-1} s^{-1}) vs temperature for the barrierless phenyl and vinyl + O_2 and phenoxy and vinoxy + O association reactions. Solid lines indicate empirical three-parameter Arrhenius fits of the calculated rate constants.

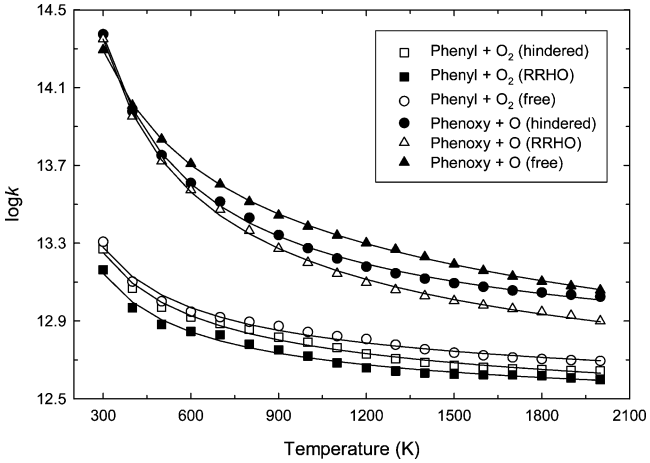

Figure 10. Calculated high-pressure limit rate constants (k, cm^3 mol^{-1} s^{-1}) vs temperature for the barrierless phenyl + O_2 and phenoxy + O association reactions, with treatment of the C−OO internal rotational mode as a hindered rotor (hindered), as a vibrational frequency (RRHO), and as a free rotor (free). Solid lines indicate empirical three-parameter Arrhenius fit of the calculated rate constants.

Comparison to Experimental Data. As noted in the Introduction, there exist two measurements (to our knowledge) of the phenyl + O_2 association rate constant, those of Yu and Lin[16] and those of Schaugg et al.[17] Our calculated rate constant for the phenyl + O_2 reaction is compared to these experimental results in Figure 13. We found that our calculated rate expression is in good agreement with the measurements of both Schaugg et al. and Yu and Lin, in both cases being within an order of magnitude. Our results exhibit a small negative temperature dependence, similar to the findings of Yu and Lin. The results of Yu and Lin are considered to be at or near the high-pressure limit and should therefore provide a direct comparison to our calculations, assuming no reverse reaction to phenyl + O_2.

A number of experimental results exist for the vinyl radical + O_2 reaction, with which to make a comparison to our calculated rate constant. These experimental results are at low pressures and will therefore suffer from falloff effects, decreasing the rate of reaction. Falloff effects increase with decreasing pressure and increasing temperature. The experimental results also include the unobservable reverse reaction to vinyl + O_2, potentially further decreasing the observed reaction rate; our calculated rate constants do not include reverse dissociation of the energized adducts. Figure 14 shows a comparison between the calculated and the experimental values of the vinyl + O_2 rate constant, and we find that our calculations provide an upper limit to the experimental measurements. Disagreement is greatest at lower temperatures, where the calculated rate constants experience less falloff. This may indicate that formation of the van der Waals well is becoming the rate-limiting process, with our results overestimating the reaction rate constant. We stress, however, that we are generally interested in these reactions at temperatures relevant to combustion and ignition systems, where agreement between calculated and experimental values is very satisfactory.

Fewer results, either experimental or theoretical, are available for the phenoxy and vinoxy + O association reactions. The phenoxy + O association can occur at the oxyl radical site, as studied here, or at an ortho or para site on the ring; these later reactions yield the *o*-semiquinone and *p*-semiquinone radicals, respectively. Oxygen atom addition at the oxyl site is expected

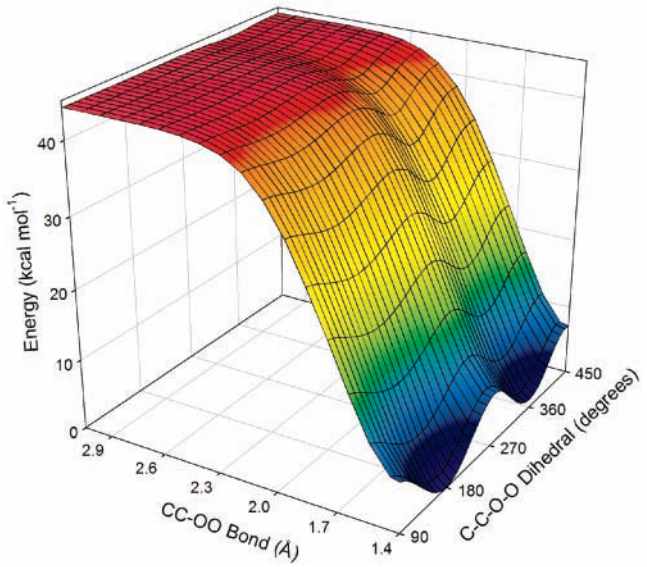

Figure 11. Three-dimensional potential energy surface for the barrierless vinyl + O_2 → vinylperoxy reaction. Reaction channels to both *cis*- and *trans*-vinylperoxy are depicted.

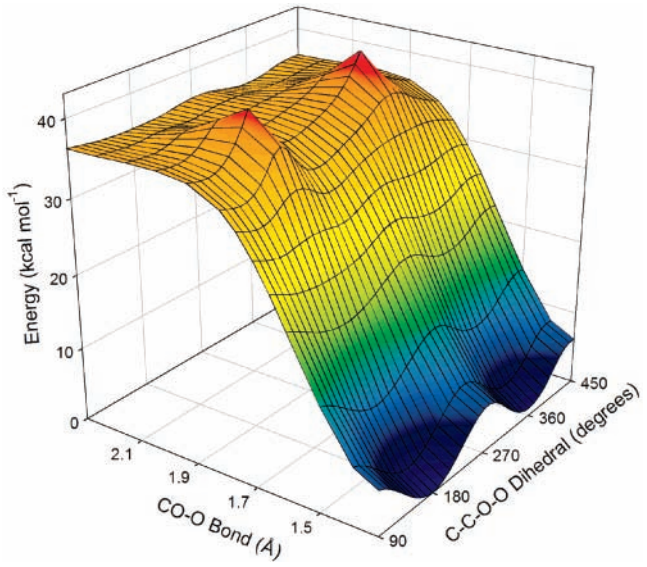

Figure 12. Three-dimensional potential energy surface for the barrierless vinoxy + O → vinylperoxy reaction. Reaction proceeds through a gauche transition state to *trans*-vinylperoxy.

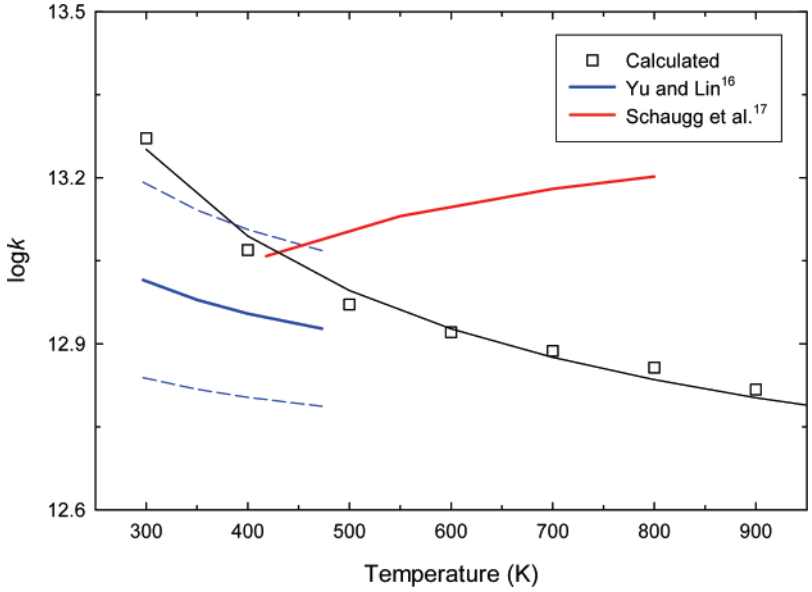

Figure 13. Comparison between calculated (high-pressure limit) and experimental rate constants (k, cm^3 mol^{-1} s^{-1}) for the phenyl + O_2 association reaction. Solid black line indicates empirical three-parameter Arrhenius fit of the calculated rate constants. Dashed lines indicate uncertainty in the measurements of Yu and Lin.[16]

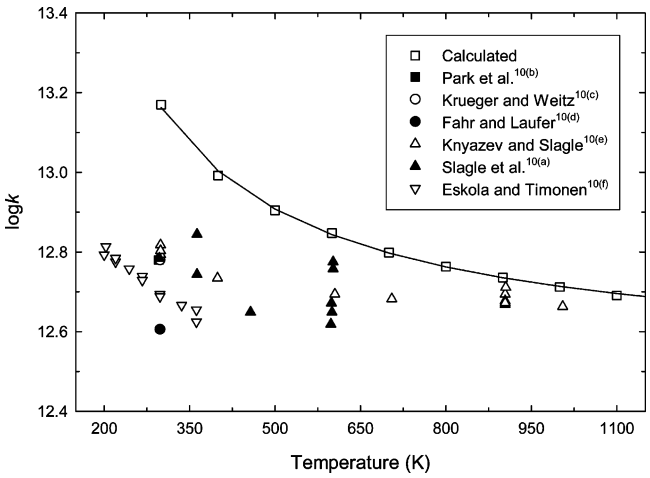

Figure 14. Comparison between calculated (high-pressure limit) and experimental rate constants (k, cm^3 mol^{-1} s^{-1}) for the vinyl + O_2 association reaction. Solid line indicates empirical three-parameter Arrhenius fit of the calculated rate constants.

to yield the products phenyl + O_2, stabilized phenylperoxy radical, and a series of unsaturated (oxy-)hydrocarbon ring compounds and ring opening products. Lin and Mebel[26] studied the ortho site phenoxy + O addition mechanism using ab initio techniques and reported k [cm^3 molecule^{-1} s^{-1}] = $5.52 \times 10^{-17} T^{1.38} \exp(148/T)$ for $T = 300 - 3000$ K (the oxyl addition mechanism was deemed to be unimportant). Buth et al.[27] measured the total rate of the phenoxy + O reaction, using a discharge flow reactor. The major reaction products were benzoquinone + H, with smaller amounts of C_5H_5 + CO_2. We assume that benzoquinone + H was formed from the *o*- and *p*-semiquinone radicals and is the sum of *o*- and *p*-benzoquinone. C_5H_5 + CO_2 are assumed to be the product of oxyl O addition, followed by O insertion into the C_6 ring, followed by ring contraction and CO_2 elimination. Using the C_2H_5 + O reaction as a reference, a rate constant of 1.68×10^{14} cm^3 mol^{-1} s^{-1} was deduced for the total phenoxy + O reaction at 295 K. With a branching ratio of less than 15% to the C_5H_5 + CO_2 channel, this gives a rate constant of at least 1.43×10^{14} cm^3 mol^{-1} s^{-1} for the ring addition pathways and less than 2.52×10^{13} cm^3 mol^{-1} s^{-1} for the oxyl addition mechanism (this assumes that C_5H_5 and CO_2 are the only major products of the oxyl O addition reaction). Rate constants for the latter pathway agree well with our calculated phenoxy + O rate constant (9.1×10^{12} cm^3 mol^{-1} s^{-1} at 300 K), but there is around a 3 orders of magnitude difference to the ring addition rate constant of Lin and Mebel (300 K, ortho only), and further work is obviously required to better identify this rate constant.

Rate constants for O−O bond dissociation in the vinylperoxy and phenylperoxy radicals, when fit to a simple two-parameter Arrhenius equation, yield pre-exponential factors (A) of 9×10^{13} and 2×10^{14} s^{-1}, with activation energies (E_a) of 32.1 and 32.9 kcal mol^{-1}, respectively. This shows a small increase in A with increasing reaction endothermicity. This is not unexpected, as the Hammond postulate suggests that the transition state should become more product-like (i.e., looser) with increasing reaction barrier. Comparing our results to O−O bond dissociation in the ethylperoxy radical (CH_3CH_2OO),[28] we find that this trend continues. Here, a two-parameter Arrhenius fit yields $A = 1 \times 10^{15}$ s^{-1} and $E_a = 61.5$ kcal mol^{-1}. The near-doubling of the reaction barrier is seen to result in an order of magnitude increase in A. There is a second explanation for this change in the pre-exponential factor with the different reaction energies of the alkyl versus phenyl or vinyl radical systems. The lower pre-exponential factors in the vinyl and phenyl systems can be explained by reactions being β scission reactions, where in the alkyl systems there is no carbonyl π bond that can be formed. The reaction is more like a simple dissociation in the alkyl-peroxy dissociations to the alkoxy plus oxygen atom.

These results may be useful in estimating rate constants for O−O dissociation in other hydrocarbons, as we observe an almost linear increase in A with E_a (or ΔH_{rxn}), according to $A = 5.63 \times 10^{13} E_a - 1.98 \times 10^{15}$. We caution that interpolation, and especially extrapolation, based upon this relationship may lead to very large errors, due to the minimal number of data points used in its derivation. This is especially pertinent at low reaction enthalpies, where a discrete (i.e., non-variational) transition state structure might be reasonably expected. However, further work developing correlations such as this certainly is warranted.

Conclusion

The barrierless phenyl and vinyl + O_2 and phenoxy and vinoxy + O reactions were studied using variational transition state theory, with O3LYP/6-31G(d) potentials scaled by G3B3 reaction enthalpies. Full hindered internal rotor analysis was provided for rotation about the R−OO bond in all systems. Both of the O_2 addition reactions show loose transition state structures, and calculated rate constants for association are in relatively good agreement with experimental values. In the phenyl system, treatment of the R−OO internal rotor as a hindered rotation, free rotation, or vibrational frequency also was provided. The O atom addition reactions demonstrate tighter transition states, with less variation in the structure with temperature. Additional research is required on the phenoxy + O association process, to assay the relative importance of the oxyl addition mechanism (studied here) and the ortho and para ring additions. Three-dimensional PES analysis illustrates that the vinyl + O_2 reaction occurs via two discrete channels, one to *cis*-vinylperoxy and one to *trans*-vinylperoxy. The vinoxy + O reaction, however, exhibits two degenerate pathways to the *trans*-vinylperoxy radical only.

Acknowledgment. We thank the ExxonMobil educational fund and the New Jersey Institute of Technology Ada C. Fritts Chair for funding.

Supporting Information Available: O3LYP energies and scaled enthalpies for phenyl and vinyl + O_2 and phenoxy and vinoxy + O PES. Rate constants as a function of position (z) and temperature (T) for vinyl + O_2 and vinoxy + O reactions. This material is available free of charge via the Internet at http://pubs.acs.org.

References and Notes

(1) Blanksby, S. J.; Ellison, G. B. *Acc. Chem. Res.* **2003**, *36*, 255.

(2) da Silva, G.; Chen, C.-C.; Bozzelli, J. W. *J. Phys. Chem. A* **2007**, *111*, 8663.

(3) Sebbar, N.; Bockhorn, H.; Bozzelli, J. W. *Int. J. Chem. Kinet.* **2008**, in press.

(4) (a) Chen, C.-C.; Bozzelli, J. W.; Farrell, J. T. *J. Phys. Chem. A* **2004**, *108*, 4632. (b) Tokmakov, I. V.; Kim, G.-S.; Kislov, V. V.; Mebel, A. M.; Lin, M. C. *J. Phys. Chem. A* **2005**, *109*, 6114. (c) Lindstedt, R. P.; Skevis, G. *Combust. Flame* **1994**, *99*, 551. (d) Merle, J. K.; Hadad, C. M. *J. Phys. Chem. A* **2004**, *108*, 8419. (e) Fadden, M. J.; Hadad, C. M. *J. Phys. Chem. A* **2004**, *104*, 8121. (f) Barckholtz, C.; Fadden, M. J.; Hadad, C. M. *J. Phys. Chem. A* **1999**, *103*, 8108. (g) Fadden, M. J.; Barckholtz, C.; Hadad, C. M. *J. Phys. Chem. A* **2000**, *104*, 3004. (h) Carpenter, B. K. *J. Am. Chem. Soc.* **1993**, *115*, 9806. (i) Mebel, A. M.; Lin, M. C. *J. Am. Chem. Soc.* **1994**, *116*, 9577. (j) Sirjean, B.; Ruiz-Lopez, M. F.; Glaude, P. A.; Battin-Leclerc, F.; Fournet, R. *Proc. Eur. Combust. Meet.* **2005**.

(5) (a) Sebbar, N.; Bockhorn, H.; Bozzelli, J. W. *Proc. Eur. Combust. Meet.* **2003**, *26*. (b) Sebbar, N.; Bozzelli, J. W.; Bockhorn, H. *Int. J. Chem. Kinet.* **2005**, *37*, 633. (c) Sebbar, N.; Bockhorn, H.; Bozzelli, J. W. *J. Phys. Chem. A* **2005**, *109*, 2233. (d) Altarawneh, M.; Dlugogorski, B. Z.; Kennedy, E. M.; Mackie, J. C. *J. Phys. Chem. A* **2006**, *110*, 13560.

(6) (a) Lovell, A. B.; Brezinsky, K.; Glassman, I. *Int. J. Chem. Kinet.* **1989**, *21*, 547. (b) Colussi, A. J.; Zabel, F.; Benson, S. W. *Int. J. Chem. Kinet.* **1977**, *9*, 161.

(7) da Silva, G.; Chen, C.-C.; Bozzelli, J. W. *Chem. Phys. Lett.* **2006**, *424*, 42.

(8) (a) Karasek, F. W.; Dickson, L. C. *Science (Washington, DC, U.S.)* **1987**, *237*, 754. (b) Khachatryan, L.; Asatryan, R.; Dellinger, B. *Chemosphere* **2003**, *52*, 695. (c) Khachatryan, L.; Asatryan, R.; Dellinger, B. *J. Phys. Chem. A* **2004**, *108*, 9567. (d) Asatryan, R.; Davtyan, A.; Khachatryan, L.; Dellinger, B. *J. Phys. Chem. A* **2005**, *109*, 11198. (e) Altarawneh, M.; Dlugogorski, B. Z.; Kennedy, E. M.; Mackie, J. C. *J. Phys. Chem. A* **2007**, *111*, 2563.

(9) (a) Dellinger, B.; Pryor, W. A.; Cueto, R.; Squadrito, G. L.; Hegde, V.; Deutsch, W. A. *Chem. Res. Toxicol.* **2001**, *14*, 1371. (b) Dellinger, B.; Lomnicki, S.; Khachatryan, L.; Maskos, Z.; Hall, R. W.; Adounkpe, J.; McFerrin, C.; Truong, H. *Proc. Combust. Inst.* **2007**, *31*, 521.

(10) (a) Slagle, I. R.; Park, J.-Y.; Heaven, M. C.; Gutman, D. *J. Am. Chem. Soc.* **1984**, *106*, 4356. (b) Park, J.-Y.; Heaven, M. C.; Gutman, D. *Chem. Phys. Lett.* **1984**, *104*, 469. (c) Krueger, H.; Weitz, E. *J. Chem. Phys.* **1988**, *88*, 1608. (d) Fahr, A.; Laufer, A. H. *J. Phys. Chem.* **1988**, *92*, 7229. (e) Knyazev, V. D.; Slagle, I. R. *J. Phys. Chem.* **1995**, *99*, 2247. (f) Eskola, A. J.; Timonen, R. S. *Phys. Chem. Chem. Phys.* **2003**, *5*, 2557. (g) Yang, R.; Yu, L.; Jin, X.; Zhou, M.; Carpenter, B. K. *J. Chem. Phys.* **2005**, *122*, 14511.

(11) (a) Westmoreland, P. R. *Combust. Sci. Technol.* **1992**, *82*, 151. (b) Carpenter, B. K. *J. Am. Chem. Soc.* **1993**, *115*, 9806. (c) Klippenstein, S. J.; Georgievskii, Y.; Miller, J. A.; Nummela, J. A.; Carpenter, B. K.; Westmoreland, P. R. Proceedings of the 3rd Joint Meeting of the U.S. Sections of the Combustion Institute, Chicago, IL, March 17−19, 2003. (d) Carpenter, B. K. *J. Phys. Chem.* **1995**, *99*, 9801. (e) Mebel, A. M.; Diau, E. W. G.; Lin, M. C.; Morokuma, K. *J. Am. Chem. Soc.* **1996**, *118*, 9759. (f) Chang, A. Y.; Bozzelli, J. W.; Dean, A. M. *Zeit. Phys. Chem.* **2000**, *11*, 1533. (g) Li, L.; Deng, P.; Wang, X.; Tian, A. *J. Mol. Struct.* **2002**, *588*, 211. (h) Mebel, A. M.; Kislov, V. V. *J. Phys. Chem. A* **2005**, *109*, 6993. (i) Hua, H.; Ruscic, B.; Wang, B. *Chem. Phys.* **2005**, *311*, 335.

(12) da Silva, G.; Kim, C.-H.; Bozzelli, J. W. *J. Phys. Chem. A* **2006**, *110*, 792512.

(13) (a) Cavallotti, C.; Rota, R.; Carrà, S. *J. Phys. Chem. A* **2002**, *106*, 7769. (b) Richter, H.; Howard, J. B. *Phys. Chem. Chem. Phys.* **2002**, *4*, 2038.

(14) da Silva, G.; Sebbar, N.; Bozzelli, J. W. *J. Phys. Chem. A* **2006**, *110*, 13058.

(15) da Silva, G.; Bozzelli, J. W.; Liang, L.; Farrell, J. T. Proceedings of the 5th U.S. Combustion Meeting, San Diego, CA, March 25−28, 2007.

(16) Yu, T.; Lin, M. C. *J. Am. Chem. Soc.* **1994**, *116*, 9571.

(17) Schaugg, J.; Tranter, R. S.; Grotheer, H.-H. Proceedings of the 8th International Symposium on Transport Phenomena in Combustion, San Francisco, CA, July 16−20, 1995.

(18) For example, see: (a) Klippenstein, S. J.; Georgievskii, Y.; Harding, L. B. *Phys. Chem. Chem. Phys.* **2006**, *6*, 1133. (b) Georgievskii, Y.; Klippenstein, S. J. *J. Phys. Chem. A* **2007**, *111*, 3802. (c) Sabbah, H.; Biennier, L.; Sims, I. R.; Georgievskii, Y.; Klippenstein, S. J.; Smith, I. W. M. *Science (Washington, DC, U.S.)* **2007**, *317*, 102.

(19) (a) Handy, N. C.; Cohen, A. J. *Mol. Phys.* **2001**, *99*, 403. (b) Cohen, A. J.; Handy, N. C. *Mol. Phys.* **2001**, *99*, 607.

(20) (a) Guner, V. A.; Khuong, K. S.; Houk, K. N.; Chuma, A.; Pulay, P. *J. Phys. Chem. A* **2004**, *108*, 2959. (b) Baker, J.; Pulay, P. *J. Chem. Phys.* **2002**, *117*, 1441. (c) Baker, J.; Pulay, P. *J. Comput. Chem.* **2003**, *24*, 1184.

(21) Baboul, A. G.; Curtiss, L. A.; Redfern, P. C.; Raghavachari, K. *J. Chem. Phys.* **1999**, *110*, 7650.

(22) Frisch, M. J.; Trucks, G. W.; Schlegel, H. B.; Scuseria, G. E.; Robb, M. A.; Cheeseman, J. R.; Montgomery, J. A., Jr.; Vreven, T.; Kudin, K. N.; Burant, J. C.; Millam, J. M.; Iyengar, S. S.; Tomasi, J.; Barone, V.; Mennucci, B.; Cossi, M.; Scalmani, G.; Rega, N.; Petersson, G. A.; Nakatsuji, H.; Hada, M.; Ehara, M.; Toyota, K.; Fukuda, R.; Hasegawa, J.; Ishida, M.; Nakajima, T.; Honda, Y.; Kitao, O.; Nakai, H.; Klene, M.; Li, X.; Knox, J. E.; Hratchian, H. P.; Cross, J. B.; Adamo, C.; Jaramillo, J.; Gomperts, R.; Stratmann, R. E.; Yazyev, O.; Austin, A. J.; Cammi, R.; Pomelli, C.; Ochterski, J. W.; Ayala, P. Y.; Morokuma, K.; Voth, G. A.; Salvador, P.; Dannenberg, J. J.; Zakrzewski, V. G.; Dapprich, S.; Daniels, A. D.; Strain, M. C.; Farkas, O.; Malick, D. K.; Rabuck, A. D.; Raghavachari, K.; Foresman, J. B.; Ortiz, J. V.; Cui, Q.; Baboul, A. G.; Clifford, S.; Cioslowski, J.; Stefanov, B. B.; Liu, G.; Liashenko, A.; Piskorz, P.; Komaromi, I.; Martin, R. L.; Fox, D. J.; Keith, T.; Al-Laham, M. A.; Peng, C. Y.; Nanayakkara, A.; Challacombe, M.; Gill, P. M. W.; Johnson, B.; Chen, W.; Wong, M. W.; Gonzalez, C.; Pople, J. A. *Gaussian 03*, Revision D.01; Gaussian, Inc.: Pittsburgh, PA, 2004.

(23) Mokrushin, V.; Bedanov, V.; Tsang, W.; Zachariah, M.; Knyazev, V. *ChemRate*, Version 1.5.2; National Institute of Standards and Testing: Gaithersburg, MD, 2006.

(24) Pitzer, K. S. *J. Chem. Phys.* **1946**, *14*, 239.

(25) Pitzer, K. S.; Gwinn, W. D. *J. Chem. Phys.* **1942**, *10*, 428.

(26) Lin, M. C.; Mebel, A. M. *J. Phys. Org. Chem.* **1995**, *8*, 407.

(27) Buth, R.; Hogermann, K.; Seeba, J. *Symp. (Int.) Combust., [Proc.]* **1994**, 841.

(28) Sheng, C. Y.; Bozzelli, J. W.; Dean, A. M.; Chang, A. Y. *J. Phys. Chem. A* **2002**, *106*, 7276.